

Hemodynamic Assessment of Pre- and Post-operative Aortic Coarctation from MRI

Kristóf Ralovich^{1,2}, Lucian Itu^{2,3}, Viorel Mihalef², Puneet Sharma²,
Razvan Ionasec², Dime Vitanovski^{2,4}, Waldemar Krawtuschuk^{2,4},
Allen Everett⁵, Richard Ringel⁵, Nassir Navab¹, and Dorin Comaniciu²

¹ Technical University of Munich, Germany

² Siemens Corporation, Corporate Research and Technology, USA

³ Transilvania University of Brasov, Romania

⁴ Friedrich-Alexander University Erlangen-Nuremberg, Germany

⁵ The Johns Hopkins Hospital, USA

Abstract. Coarctation of the aorta (CoA), is a congenital defect characterized by a severe narrowing of the aorta, usually distal to the aortic arch. The treatment options include surgical repair, stent implantation, and balloon angioplasty. In order to evaluate the physiological significance of the pre-operative coarctation and to assess the post-operative results, the hemodynamic analysis is usually performed by measuring the pressure gradient (ΔP) across the coarctation site via invasive cardiac catheterization. The measure of success is reduction of the ($\Delta P > 20mmHg$) systolic blood pressure gradient. In this paper, we propose a non-invasive method based on Computational Fluid Dynamics and MR imaging to estimate the pre- and post-operative hemodynamics for both native and recurrent coarctation patients. High correlation of our results and catheter measurements is shown on corresponding pre- and post-operative examination of 5 CoA patients.

1 Introduction

Coarctation of the aorta (CoA) accounts for 5 – 8% of the 8/1,000 congenital heart disease (that is 4–6/10,000) live births [1] in the USA. CoA is a congenital defect characterized by a severe narrowing of the aorta, usually distal to the aortic arch. Patients born with CoA require lifelong medical/surgical care, that includes invasive and non-invasive imaging, drug therapy and if the CoA recurs, invasive catheterization or surgical intervention to reduce the blood pressure in the ascending aorta.

Pre-operative evaluation of CoA severity relies predominately on non-invasive arm/leg blood pressure gradients or if anatomy makes that comparison not feasible, estimation by Doppler ultrasonography. The clinical gold-standard is obtained by invasive cardiac catheterization to measure (ΔP) across the coarctation site. Recently, Doppler and phase contrast (PC) MRI based methods have been proposed for a non-invasive estimation of ΔP [2] by using simplified

relationships (e.g. modified Bernoulli equation) between flow and pressure. However, such approaches often overestimate the pressure difference and do not provide other hemodynamic parameters (such as wall-shear stress, vorticity, etc.) that characterize the complex flow-field associated with CoA, which could potentially be used for diagnosis and treatment planning.

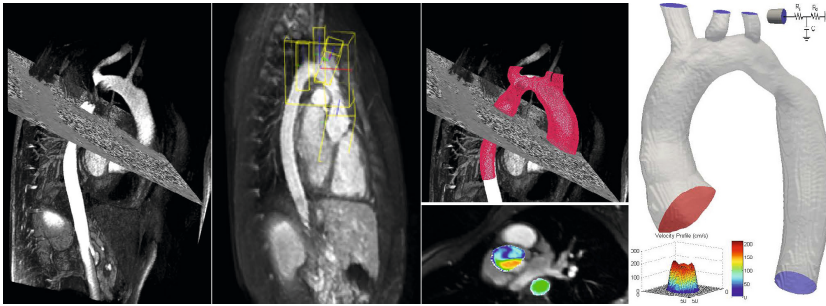


Fig. 1. **Left:** Overlay of angiogram and PC-MRI **Left Middle:** Bounding boxes for parts of the vessel tree, retrieved by learning based detection **Right Middle:** Segmented vessel tree and delineated aortic flow profiles **Right:** Overview of boundary conditions applied, measured flow profile at AAo, Windkessel model at carotid and descending outlets

Multiple groups have investigated CoA hemodynamics through simulation. Coupling the aorta with a lumped parameter model of the left ventricle, [3] applies realistic inflow boundary conditions, but only studies two patients. Outlet conditions are treated in [4], but employing simple heuristics at the supra aortic branches, also pre-operative simulation is not compared with post repair of the same patient. [5] applies detailed boundary conditions and accurate simulation procedure, but imaging data was specifically acquired for the study, and potentially difficult to reproduce in standard exams.

To address these issues, we propose an MR image-based pre-processing and hemodynamics simulation pipeline for thoracic aortic investigation. A patient-specific model of the aorta and supra-aortic arteries is automatically estimated using a discriminative learning-based method. Based on the lumen geometry, we introduce a CFD setup employing personalized boundary conditions. The simulation provides dense 3D+time velocity and pressure maps. We applied the method to existing data of CoA patients of multiple hospitals enrolled in a FDA authorized clinical trial [1]. Blood pressure computation is validated against invasive catheterization on 5 cases. Strengths of our method are 1) end-to-end computational pipeline that may be integrated within the clinical workflow, 2) the ability to work on clinical images acquired within existing protocols and 3) reproducible simulation results of good initial agreement.

2 Proposed Method

2.1 Estimation of the Patient-Specific Lumen

An accurate geometrical representation of the lumen boundaries is essential for subsequent simulations. To facilitate reproducibility of our computation, we developed a robust learning-based method to estimate a model of the aorta and supra-aortic arteries from contrast enhanced MR angiograms (CE-MRA). The thoracic aorta and main branches are represented as multiple parts: aortic root, aortic arch, walls of ascending and descending aorta, and the supra-aortic arteries (SAoA) - brachiocephalic trunk, left common carotid artery, left subclavian artery (illustrated on Fig. 1, **Left Middle**).

In a first step, the pose of each part is estimated following a hierarchical scheme that allows for the utilization of anatomical constraints. In image I , each pose θ is parametrized as a 3D affine transformation. We formulate the estimation as a multi-object detection problem and learn the posterior probability $p(\theta|I)$ using the Probabilistic Boosting Tree [6]. As the aortic arch pose estimation produced most accurate results, we exploit its anatomical proximity to the SAoA, and constrain the pose estimation of the former by learning the variation in their relative distances from the available training set. Constrained by the estimated poses, each part is initialized with a corresponding mean model constructed by employing statistical shape analysis [7]. A lumen detector is trained using the PBT and Haar-like features to drive the deformation of the initial model towards the actual boundary in the image. The final model is obtained by merging the separately estimated parts using a sequence of forward and backward projection to/from Eulerian representation to retrieve the composited Lagrangian arterial tree geometry.

2.2 Estimation of the Patient-Specific Blood Flow from PC-MRI

To quantify the subject's measured blood flow conditions, patient-specific flow profiles over the entire cardiac cycle are extracted at the aortic in- and outflow from the velocity encoded 2D PC-MRI Cine images. These sequences contain through-plane blood flow measurements in an oblique arrangement, intersecting the aorta twice: at the ascending aorta (AAo) above the valve and in the region of the descending aorta (DAo). Given a centerline of the aorta calculated from the segmentation, delineation of the lumen boundary on the MR image is initialized using graph cuts, and physiological radii constraints. The single time point segmentation is then tracked throughout the cardiac cycle similar to [8]. Inside each patch, sampling of the PC-MR image is performed at the pixel centers to obtain velocity values over the entire cardiac cycle. This velocity field is integrated over the area of the segmented contour to estimate the aortic blood flow rate.

2.3 Non-invasive Estimation of Personalized Boundary Conditions

In order to perform a patient-specific simulation, the inlet and outlet boundary conditions are personalized based on the non-invasive measurements. Given the high computational cost associated with unsteady 3D flow simulations, we use an axisymmetric reduced-order model of aortic hemodynamics for a quick estimation of patient-specific parameters that are subsequently used for a personalized 3D flow simulation.

The inlet boundary condition is specified by imposing the time-varying flow rate in the ascending aorta obtained from the PC-MRI data. For the outlet boundary condition, we use a 3-element Windkessel model to specify the downstream resistance and compliance of the vessels that are not explicitly modeled in the flow computations. At each of the four outlets (SAoA and DAo), the windkessel model consists of two resistances (R_p and R_d) and one compliance (C). R_p is proximal resistance, R_d the distal resistance and C the total compliance of the downstream circulation for each outlet. At each outflow, the total resistance R_t , (where $R_t = R_p + R_d$) is estimated from the mean arterial pressure (P_{MA}) and average flow (Q) by using the relation: $R_t = \frac{P_{MA}}{Q}$. For the non-invasive estimation of P_{MA} in the AAo, we use the systolic and diastolic cuff pressures, together with the heart rate: $P_{MA} = P_{DB} + \left[\frac{1}{3} + (Hr \cdot 0.0012)\right] (P_{SB} - P_{DB})$, where P_{DB} and P_{SB} are the diastolic and systolic blood pressures and Hr is the heart rate.

The average flows at the ascending (Q_{AAo}) and the descending aorta (Q_{DAo}) are obtained from the PC-MRI data. Hence, the total flow in the three remaining outflow vessels (Q_{up}) can be obtained by: $Q_{up} = Q_{AAo} - Q_{DAo}$. As has been shown previously [9], the total flow in the first few branches, starting from the aortic root, is distributed proportionally to the square of the vessel radius, i.e. $Q_i = \frac{Q_{up} \cdot r_i^2}{\sum_{i=1}^3 r_i^2}$ where r_i is the vessel radius at the outflow of upper branch i . Since the pressure difference between the ascending aorta and the three upper branches is insignificant, we use the same average pressure to estimate the total resistance at each upper outlet branch: $(R_t)_i = \frac{P_{MA}}{Q_i}$. For the descending aorta, the assumption that P_{MA} is the same as for the ascending aorta does not hold true, since the coarctation induces a significant pressure drop. The coarctation introduces a flow-dependent resistance ($R_s(Q)$) and thus, the total resistance, which represents the sum of the resistance of the coarctation and of the outflow model, is estimated as follows: $(R_t)_{DAo} + R_s(Q) = \frac{P_{MA}}{Q_{DAo}}$. The resistance of the coarctation is estimated with a semi-empirical model: $R_s(Q) = \frac{\mu \cdot K_v}{2 \cdot \pi \cdot r_0^3} + \frac{\rho \cdot K_t}{2 \cdot A_0^2} \left(\frac{A_0}{A_s} - 1\right)^2 Q_{DAo}$ where r_0 is the proximal radius of the coarctation, A_0 and A_s are the proximal and minimum cross-sectional areas, μ is the dynamic viscosity, ρ is the blood density and K_v and K_t are two constants which represent the viscous and turbulent losses of energy. Q_{DAo} , the measured average flow rate through the descending aorta. Using the last two equations the total resistance at the descending aorta is then computed. After the computation of the total resistances, the last step is to compute R_p and R_d . R_p at each outflow is equal to the characteristic resistance of the vessel (in order to minimize the reflections),

which is computed by the expression $(R_p)_i = \frac{1}{H \cdot r_i^2} \sqrt{\frac{2 \cdot \rho \cdot E \cdot h}{3 \cdot r_i}}$, as described in [10]. R_d is then computed by $R_d = R_t - R_p$. For estimating the total compliance we use the method in [11] and redistribute the individual compliances at each outlet. Once the windkessel parameters are estimated, no further tuning is performed to run the simulations.

2.4 Patient-Specific 3D CFD Simulations

To obtain comprehensive flow information in three dimensions we solve the full 3D Navier-Stokes equations in the luminal aortic domain calculated, using the personalized outflow boundary conditions for pressure. We use an embedded boundary method for automatic transfer of the tagged STL triangular lumen mesh into a cartesian domain. The embedding function is a signed-distance function computed using the Closest Point Transform [12]. The computational domain cells are tagged based on their relation with the inlet triangular mesh as follows: *Exterior* (no computation is taking place), *Interior* (computation is taking place), *Inlet*, *Outlet* and *Wall* (appropriate boundary conditions are imposed). The *Inlet* and *Wall* cells are all interior to the domain, while the *Outlet* cells are situated on the domain boundaries, by extending the lumen of each vessel in its centerline direction [13] until it reaches the cartesian boundary. Our embedded boundary Navier-Stokes solver uses a fractional step method [14] that computes in a first step an intermediate velocity field, using the nonlinear advection-diffusion equation for velocity, and then projects the intermediate velocity onto the field of divergence free and tangent to the vessel boundary vector fields. For the velocity advection we use second-order upwind, Van-Leer slope limiting methods, while for the diffusion force components we use a semi-implicit approach as in [15] which is first order accurate and unconditionally stable in 3D. We solve the pressure projection Poisson equation using an efficient implicit multi-grid preconditioned conjugate gradient solver. The boundary conditions for the velocity are Dirichlet in the *Inlet* cells, no-slip (Dirichlet) in the *Wall* cells, and Neumann in the *Outlet* cells [16]. We use a variable-in-time flat inlet velocity profile, and outlet pressure boundary conditions provided by the axisymmetric 1D simulations. The blood density and viscosity are set to literature based values for healthy individuals ($1.05g/cm^3$ and $4mPa \cdot s$).

3 Experiments and Validation

3.1 Segmentation

The accuracy of our method is demonstrated on a set of 212 3D images with wide range of morphological and pathological variations. Data was retrospectively collected from multiple hospitals participating in the COAST Trial [1], acquired using heterogeneous MR protocols/sequences with scanners from all three major vendors. Each volume in the data set is associated with an annotation (from manual operators) which is considered as ground truth for training and testing.

The fused aortic vessel tree segmentation accuracy was evaluated by using the point-to-mesh metric (Table 1a). Average detection time for all parts is in the range of 2 – 3 minutes on an Intel Core i7 laptop.

From a clinical perspective, the quantitative capabilities of our system are demonstrated on 32 patients with aortic anomalies (age: 5-36 years, 17 with CoA and 15 with bicuspid aortic valve and dilated AAO) by comparing a set of morphological measurements[17] automatically derived from our segmentation to measurements manually performed by our cardiologist collaborators. The aortic min and max diameter were measured at five location: aortic sinus (**AS**), sino-tubular junction (**STJ**), ascending aorta (**AAO**), transverse arch (**TA**), and descending aorta (**DA**). Statistical results correlated ($p < 0.001$, $r = 0.94$) between model-based and manually measured min and max diameters. Table 1b summarizes the mean measurement errors for each segment separately.

3.2 Parameter Estimation, Simulation Results and Validation

In order to demonstrate the proposed method for non-invasive hemodynamic assessment, we investigated 5 patient datasets with native and/or recurrent coarctation that involved the aortic isthmus. The stenoses received repair through balloon angioplasty and stenting.

Using the above methods the patient-specific geometric vessel wall model and corresponding time-resolved flow profiles were estimated from MR images. To make sure that segmentation errors (e.g. results of image quality due to MR signal drop-out inside the metallic stent for post-op) do not influence the simulation outcomes, the vessel tree geometry was reviewed by a manual operator in all experiments.

Given the patient-specific anatomy, measured flow rates at the AAO and DAo, and systolic and diastolic blood pressures and heart rate, we performed a non-invasive parameter estimation of the boundary conditions for each patient. The results obtained for the non-invasive pressure gradients are summarized in Table 1c, together with the invasive pressures obtained from cardiac catheterization. The pressure differences between the AAO-DAo and TAA-DAo are determined at the time-instant when the flow rate through the descending aorta is maximal.

Table 1. **a)** Segmentation accuracy (mm) and **b)** comparison between manual and model-based clinical measurements (mm). **c)** Comparison of the pressure obtained from invasive catheterization and our proposed non-invasive method: systolic blood pressure gradients ($mmHg$) between AAO-DAo and transverse aortic arch (TAA)-DAo.

(a)			(b)			(c)			
	Mean (Std)	Median		AS	STJ	AAO	Pati	ΔP	ΔP
			min				ent	AAo-DAo	TAA-DAo
aorta	2.29 ± 1.74	1.95	max	1.61 ± 0.9	2.07 ± 1.5	1.61 ± 1.9	#1	55/58.5	53/56
brachiocephalic	3.40 ± 1.89	2.90		1.56 ± 1.3	1.28 ± 1.0	1.56 ± 1.3	#3	8/6.9	8/7.7
left common	4.59 ± 3.58	3.16					#4	30/17.3	28/24.3
left subclavian	4.64 ± 3.33	3.06	min	1.70 ± 1.2	0.8 ± 0.5		#5	14/15	18/13.2
supra-aortic	4.21 ± 2.90	3.04	max	1.34 ± 1.1	0.92 ± 0.6		#6	39/6.7	43/6.1
complete model	3.24 ± 2.32	2.49							

4 Discussion

As can be seen from the results, the proposed method performs well for most of the cases. For patients #1, #3 and #5 the simulation reproduces the catheterization within an acceptable margin. During the review of our results for case #6 we observed that an incorrect PC-MR acquisition plane (intersecting the aortic valve and left ventricular outflow tract instead of the AAO) that results in an erroneous inflow initialization, thus we just included the results for consistency. The discrepancy in #4 is due to aortic compliance as the DAo peak flow phase is delayed compared to AAO peak blood pressure.

The results from the 3D simulations for two patients are presented in Figure 2. There is a significant pressure gradient across the coarctation at peak systole, which gradually disappears towards the end of diastole. A volumetric visualization of the velocity magnitude at peak systole, late systole and end diastole are shown in the three figures at the right. The high velocity jet in the stenosis region is clearly visible as expected. Similar methodology can also be applied to the post-operative data, by taking into consideration the modified wall-stiffness introduced from the stent implantation. This is part of the ongoing work, and the preliminary results are shown in the bottom row of Figure 2. Here, the pressure gradients between AAO-DAo and TAA-DAo have been partially restored to normal values. A similar effect can also be noticed in the flow patterns: highest velocity in the aortic arch, and reduced Reynolds number.

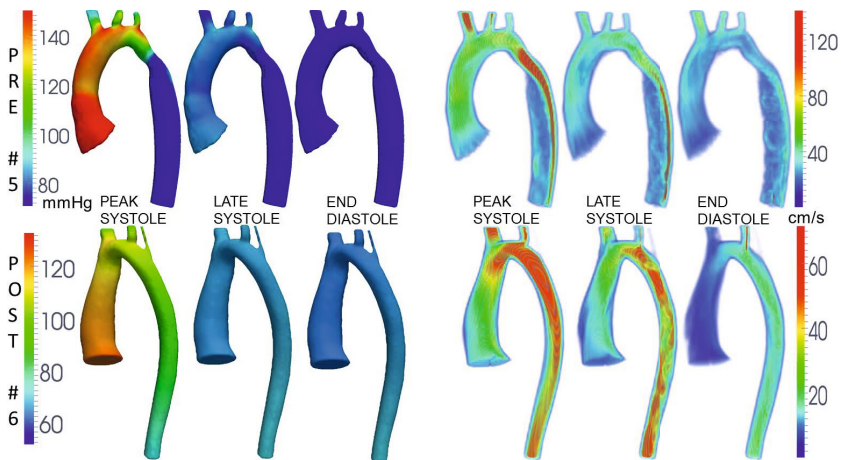


Fig. 2. Left: Blood pressure mapped on lumen boundary, Right: Volume rendered velocity magnitude (for cases pre-operative #5, post-operative #6)

Acknowledgement. This work has been partially funded by European Union project Sim-e-Child (FP7 – 248421).

References

1. Ringel, R.E., Jenkins, K.: Coarctation Of the Aorta Stent Trial (COAST) (2007)
2. Coogan, J.S., et al.: Computational fluid dynamic simulations of aortic coarctation comparing the effects of surgical- and stent-based treatments on aortic compliance and ventricular workload. *Catheterization and Cardiovascular Interventions* (2011)
3. Kim, H., Vignon-Clementel, I., Figueroa, C., LaDisa, J., Jansen, K.E.A.: On coupling a lumped parameter heart model and a three-dimensional finite element aorta model. *Annals of Biomedical Engineering* (2009)
4. Valverde, I., et al.: Predicting hemodynamics in native and residual coarctation: preliminary results of a rigid-wall computational-fluid-dynamics model (rw-cfd) validated against clinically invasive pressure measures at rest and during pharmacological stress. *Journal of Cardiovascular Magnetic Resonance* (2011)
5. LaDisa, J.F.J., Alberto Figueroa, C., Vignon-Clementel, I.E., Kim, H.J., Xiao, N., Ellwein, L.M., Chan, F.P., Feinstein, J.A., Taylor, C.A.: Computational simulations for aortic coarctation: representative results from a sampling of patients. *Journal of Biomechanical Engineering* (2011)
6. Tu, Z.: Probabilistic boosting-tree: Learning discriminative models for classification, recognition, and clustering. In: *Proc. ICCV*, vol. 2 (2005)
7. Yefeng, Z., et al.: Four-chamber heart modeling and automatic segmentation for 3-d cardiac ct volumes using marginal space learning and steerable features. *IEEE Transactions on Medical Imaging* (2008)
8. Jolly, M.P., Guetter, C., Guehring, J.: Cardiac segmentation in mr cine data using inverse consistent deformable registration. In: *ISBI* (2010)
9. Zamir, M., Sinclair, P., Wonnacott, T.H.: Relation between diameter and flow in major branches of the arch of the aorta. *Journal of Biomechanics* (1992)
10. Olufsen, M.S., Peskin, C.S., Kim, W.Y., Pedersen, E.M., Nadim, A., Larsen, J.: Numerical simulation and experimental validation of blood flow in arteries with structured-tree outflow conditions. *Annals of Biomedical Engineering* 28 (2000)
11. Stergiopoulos, N., Westerhof, B.E., Westerhof, N.: Total arterial inertance as the fourth element of the windkessel model. *American Journal of Physiology* (1999)
12. Mauch, S.: Efficient algorithms for solving static Hamilton-Jacobi equations. PhD Thesis (2003)
13. Ralovich, K., Ionasec, R., Mihalef, V., Sharma, P., Georgescu, B., Everett, A., et al.: Computational fluid dynamics framework for large-scale simulation in pediatric cardiology. In: *Computational Biomechanics for Medicine VI* (2011)
14. Bell, J.B., Colella, P., Glaz, H.M.: A second-order projection method for the incompressible Navier-Stokes equations. *J. Comput. Phys.* (1989)
15. Li, J., Renardy, Y., Renardy, M.: Numerical simulation of breakup of a viscous drop in simple shear flow through a volume-of-fluid method. *Phys. Fluids* (2000)
16. Mihalef, V., Ionasec, R.I., Sharma, P., Georgescu, B., Voigt, I., et al.: Patient-specific modelling of whole heart anatomy, dynamics and haemodynamics from four-dimensional cardiac ct images. In: *Interface Focus*. (2011)
17. Pasqua, A., et al.: Comparison of contrast and noncontrast magnetic resonance angiography for quantitative analysis of thoracic arteries in young patients with congenital heart defects. *Ann. Pediatr. Cardiology* 4(1) (2011)